

A STRAIGHTFORWARD GRADIENT-BASED APPROACH FOR HIGH-Tc SUPERCONDUCTOR DESIGN: LEVERAGING DOMAIN KNOWLEDGE VIA ADAPTIVE CONSTRAINTS

Akihiro Fujii^{*1}, Anh Khoa Augustin Lu^{1,2}, Koji Shimizu³, and Satoshi Watanabe¹

¹Department of Materials Engineering, The University of Tokyo

²National Institute for Materials Science (NIMS)

³National Institute of Advanced Industrial Science and Technology (AIST)

** Corresponding author: akihiro.fujii@cello.t.u-tokyo.ac.jp*

Abstract

Materials design aims to discover novel compounds with desired properties. However, prevailing strategies face critical trade-offs. Conventional element-substitution approaches readily and adaptively incorporate various domain knowledge but remain confined to a narrow search space. In contrast, deep generative models efficiently explore vast compositional landscapes, yet they struggle to flexibly integrate domain knowledge. To address these trade-offs, we propose a gradient-based material design framework that combines these strengths, offering both efficiency and adaptability. In our method, chemical compositions are optimised to achieve target properties by using property prediction models and their gradients. In order to seamlessly enforce diverse constraints—including those reflecting domain insights such as oxidation states, discretised compositional ratios, types of elements, and their abundance, we apply masks and employ a special loss function, namely the integer loss. Furthermore, we initialise the optimisation using promising candidates from existing dataset, effectively guiding the search away from unfavourable regions and thus helping to avoid poor solutions. Our approach demonstrates a more efficient exploration of superconductor candidates, uncovering candidate materials with higher critical temperature than conventional element-substitution and generative models. Importantly, it could propose new compositions beyond those found in existing databases, including new hydride superconductors absent from the training dataset but which share compositional similarities with materials found in literature. This synergy of domain knowledge and machine-learning-based scalability provides a robust foundation for rapid, adaptive, and comprehensive materials design for superconductors and beyond.

Keywords Materials Design · Materials Discovery · Inverse Problem

1 Introduction

Materials design is crucial for technological innovation such as the discovery of new superconductor materials. High-temperature superconductors (HTS) are especially promising because they reduce cooling costs and enable higher magnetic fields. They are also expected to be applied in fusion power generation, electric power cables, and superconducting maglev trains [1, 2].

Exploiting physical insights—such as selection of elements based on their oxidation states and the fact that materials

with too many elements are impractical—can narrow this search, making materials design more efficient. A traditional technique in materials design is elemental substitution (i.e., doping) [3, 4, 5, 6]. In this approach, one starts with a promising host material and partially substitutes certain elements to tune the properties. Substituted elements are typically chosen based on physical insights—such as oxidation states—to ensure charge neutrality and other key constraints.

Machine learning (ML) has become a widely used approach for materials discovery, offering faster property predictions than conventional Density Functional Theory (DFT) calculations and thus enabling high-throughput screening. In the context of HTS development, some studies [7, 8, 9, 10, 11, 12, 13, 14, 15] have focused on train-

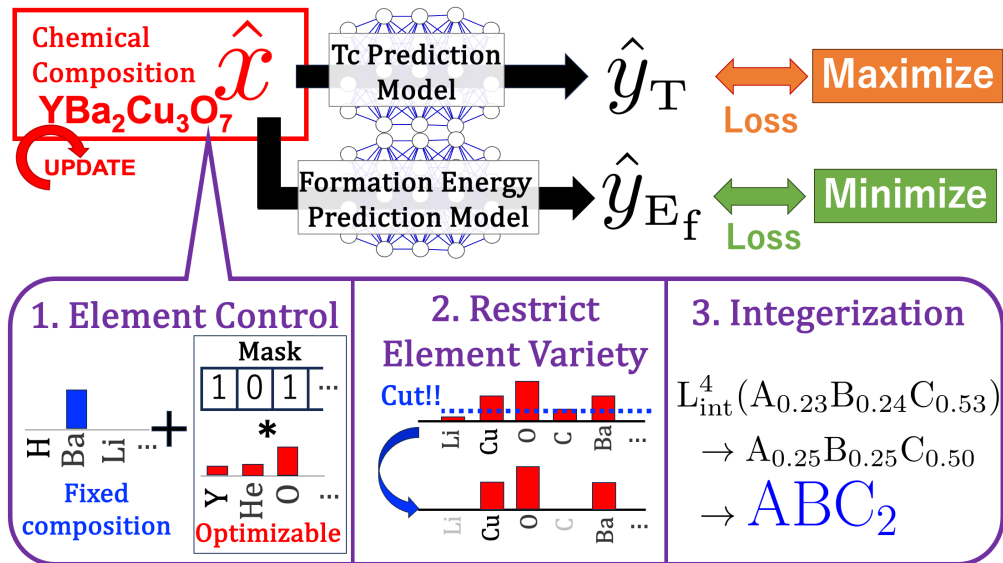


Figure 1: Overview of Knowledge-Integrated Adaptive Gradient-based Optimisation (KIAGO). KIAGO simultaneously maximises T_c and minimises the formation energy by optimising the input composition using two pretrained models and their gradients. Through the use of fixed composition vectors, masks, and specialised loss functions, KIAGO enables flexible control of the composition in three ways: **1. Element control.** Specific elements can be fixed and excluded from the optimisation target to perform conditional optimisation. KIAGO is also able to control which elements appear during the optimisation via masks. Here, we fix the composition of Barium and exclude Helium from the optimisation using the mask; **2 Restricting the maximum number of elements.** We first rank elements by their abundance in the composition and create a mask to keep only the most abundant ones up to a specified cutoff. All other elements are set to zero, ensuring that the total number of elements never exceeds the chosen limit. In this figure, we select the three most abundant elements to build a mask, which then restricts the final composition to those three elements. **3. Normalising the compositional ratios to small integers.** Here, we use the loss function L^4_{int} to guide the normalised composition to a composition consisting of four atoms.

ing superconducting transition temperature (T_c) prediction models using the SuperCon dataset [16], which comprises a large set of known superconductors.

Recently, deep generative models have gained prominence in materials design [17, 18, 19, 20], including the quest to discover novel superconductors [21, 22]. These models propose new compounds by learning the statistical distribution of existing data, thus enabling the exploration of a vast chemical space. Several studies [23, 24] employ diffusion models [25]—a deep generative model widely used in the computer vision field [26]—to generate superconductor candidates. SuperDiff [24], a diffusion model for superconductors, generates candidate superconductors by gradually removing noise from a noisy composition. Moreover, SuperDiff can generate conditioned outputs based on reference compounds using Iterative Latent Variable Refinement (ILVR) [27]. While conventional generative methods only explore materials within existing databases, SuperDiff can generate new materials based on promising reference compounds.

Moreover, there are strategies that guide deep generative models toward desired properties, such as label-based conditional generation [28], Universal Guidance [29] (UG), Classifier Guidance (CG) [30] and Classifier-Free Guid-

ance (CFG) [31]. While CG and UG use a separate property predictor to steer the generation process, CFG does not require such a predictor. Although the label-based conditional generation and CFG have both been extensively validated in image generation, their reliance on labels within the dataset limits their flexibility in materials design. By contrast, CG can be conditioned on labels not present in the target dataset using models trained on other datasets. Xie *et al.* [17] employ a strategy similar to CG, combining a diffusion model with a formation energy prediction model. Applying CG to T_c prediction models and superconducting material generation models such as SuperDiff has the potential to enable HTS design.

A gradient-based method [32, 33, 34, 35] that uses prediction models and their gradients to optimise inputs has recently attracted attention. This method is similar to CG and UG but simpler, as it does not require training a generative model. Moreover, this method allows for more flexible and adaptive conditional optimisation [35]. While there is no study of applying this technique to composition optimisation, it could be a promising approach for materials design.

Despite these advances, significant trade-offs remain. Elemental substitution can incorporate physical knowledge but

may limit exploration to a relatively narrow search space. Deep generative models can explore a broader chemical space efficiently, yet they struggle to flexibly integrate physical knowledge—such as atomic valence constraints or converting compositional ratios to integers—in an adaptive manner. On the other hand, the gradient-based method has a risk of falling into poor solutions, though this method has the potential to introduce various physical knowledge in an adaptive manner.

In this paper, to address these issues, we adopt a gradient-based method and propose a straightforward materials-design method called Knowledge-Integrated Adaptive Gradient-based Optimisation (KIAGO). This framework combines the adaptive application of domain knowledge with computational efficiency to directly optimise chemical compositions (Fig. 1). KIAGO does not require training a deep generative model, making it more straightforward to implement. Specifically, we adopt two property prediction models—one for T_c and another for formation energy—to maximise T_c while enhancing stability, thereby proposing realistic materials. Unlike CFG and label-based conditional generation, KIAGO can optimise formation energy (which is not included in the SuperCon dataset) by using a separately trained formation energy prediction model. Additionally, by conducting an intensive search around promising materials, KIAGO mitigates the risk of being trapped at poor results. Moreover, by applying masks and a specialised loss function to enforce integer values, we can effectively embed physical insights (e.g., ensuring the retention of specific elements, oxidation states, the number of elements, or integer compositional ratios), thus providing a versatile framework that accommodates diverse constraints in adaptive manners.

To validate the effectiveness of KIAGO, we performed experiments to propose promising HTS. Our approach significantly outperformed both generative models (SuperDiff and SuperDiff with CG) and conventional elemental substitution techniques in proposing high- T_c candidates efficiently. In particular, we found that SuperDiff with CG tended to generate materials with lower T_c values because the T_c distribution in the original data constrained them. In contrast, our method proposed high- T_c candidates without being limited by the original distribution. Additionally, KIAGO could keep some part of the composition fixed while optimising others, relevantly replace elements according to their oxidation states, and maintain charge neutrality perfectly. Additionally, KIAGO proposed candidate compositions that shared the same elements as hydride superconductors reported in other literature despite their absence from the SuperCon dataset. These results highlight its potential for discovering novel materials.

2 KIAGO

2.1 Overview

Knowledge-Integrated Adaptive Gradient-Based Optimisation (KIAGO) is a gradient-based method that uses pre-trained models and their gradients to directly optimise the input representation—in this case, the normalised compositional vector of candidate materials. Rather than merely searching for compositions that yield favourable properties, KIAGO introduces three key strategies to enhance material quality and provide fine-grained control: 1. Initialisation from promising materials to mitigate the risk of being trapped at poor results; 2. Masking to control elemental types; 3. Special loss functions for conversion to integers and atomic-count constraints.

2.2 Gradient-based method

A gradient-based method can adopt any predictive model, provided the chain rule of differentiation is valid from input to output. To propose superconducting materials with high- T_c , we employ a T_c predictor f_{T_c} . We also use a formation-energy predictor f_{E_f} to propose compounds that are both high- T_c and thermodynamically feasible. We introduce a hyperparameter α and define the loss L as

$$L = -f_{T_c}(\hat{x}) + \alpha f_{E_f}(\hat{x}) \quad (1)$$

$$\hat{x}_* = \underset{\hat{x}}{\operatorname{argmin}} L. \quad (2)$$

Here, $\hat{x} \in [0, 1]^{N_{\text{elem}}}$ is a compositional vector spanning N_{elem} elements. Minimising L aims to increase T_c while lowering the formation energy. However, simple minimisation poses several issues: (1) it may converge to poor solutions, (2) it lacks control over the number and type of elements, and (3) it does not ensure integer ratios in the final composition.

2.3 Initialisation based on promising materials

To avoid converging to poor solutions, we adopt a strategy of starting the optimisation from various initial states including those corresponding to known promising materials. We can reduce this risk by focusing on the areas of existing high-performance compounds. Such a strategy goes beyond doping-like approaches that only alter part of an existing material, enabling a broader range of materials to be explored. Specifically, we perturb known superconductors by substituting elements randomly and adding new elements to the composition. This technique effectively explores the local neighbourhood of promising materials.

2.4 Controlling the types of elements present

We next control which elements appear in the composition by combining a fixed composition vector and a mask (Fig. 1-1). First, we split \hat{x} into a fixed portion x_{const} and

an optimisable portion \hat{x}_{opt} :

$$\hat{x}_{\text{opt}} \in \mathbb{R}^{N_{\text{elem}}}, x_{\text{const}} \in [0, 1]^{N_{\text{elem}}}, \sum_i x_{\text{const}}^i < 1 \quad (3)$$

$$\hat{x} = x_{\text{const}} + \sigma(\hat{x}_{\text{opt}})(1 - \sum_i x_{\text{const}}^i). \quad (4)$$

Here, σ is a normalisation function that ensures each element is non-negative and the total sum is 1. A possible approach was to use the softmax function. However, to emphasize elements that remain unused, we instead chose to use normalisation after applying Rectified Linear Unit (ReLU).

$$\sigma(x) = \frac{\text{ReLU}(x)}{\sum \text{ReLU}(x)} \quad (5)$$

Because x_{const} remains unchanged, its specified composition remains fixed during optimisation. We further introduce a mask $M_{\text{elem}} (M_{\text{elem}} \in \{0, 1\}^{N_{\text{elem}}})$ to select the allowable elements. Concretely, we set

$$\hat{x}_{\text{opt}} = \hat{x}_{\text{base}} * M_{\text{elem}}, \quad (6)$$

where $\hat{x}_{\text{base}} (\hat{x}_{\text{base}} \in \mathbb{R}^{N_{\text{elem}}})$ is a trainable parameter, and the asterisk (*) denotes element-wise multiplication. This mask enforces strict control over which elements can be used, thus guiding the optimisation toward compositions that meet specified domain constraints.

2.5 Controlling the number of element types in the composition

To achieve realistic composition, we use a mask to limit how many elements can appear in the composition (Fig. 1-2). To do this, we sort the compositional values in ascending order and create a mask $M_{\text{elem}}^{\text{max}} (M_{\text{elem}}^{\text{max}} \in \{0, 1\}^{N_{\text{elem}}})$, which sets to zero any element index beyond the allowed maximum elements $n_{\text{elem}}^{\text{max}}$.

$$\sum_{i,j} (M_{\text{elem}}^{\text{max}})_{i,j} = n_{\text{elem}}^{\text{max}} \quad (7)$$

$$\hat{x}'_{\text{opt}} = \hat{x}_{\text{opt}} * M_{\text{elem}}^{\text{max}}, \quad (8)$$

2.6 Integer loss

We construct a loss function that guides the composition into integer-compatible values during optimisation (Fig. 1-3). Such values $\{c_n^{N_{\text{unit}}}\}$ are those for which the product of the normalised composition and the unit cell size N_{unit} becomes an integer ratio. For instance, if $N_{\text{unit}} = 4$, then the feasible set $\{c_n^4\}$ is $\{0.00, 0.25, 0.50, 0.75, 1.00\}$.

The integer loss measures how far each compositional ratio of element i (\hat{x}^i) is from its nearest value in $\{c_n^{N_{\text{unit}}}\}$.

$$\{c_n^{N_{\text{unit}}}\} = \{n/N_{\text{unit}}\}_{n=0,1,\dots,N_{\text{unit}}} \quad (9)$$

$$\hat{x}^i \in \{\hat{x}^{\text{H}}, \hat{x}^{\text{He}}, \hat{x}^{\text{Li}}, \dots, \hat{x}^{N_{\text{elem}}}\} \quad (10)$$

$$L_{\text{int}}^{N_{\text{unit}}}(\hat{x}) = \sum_{i=1}^{N_{\text{elem}}} \min_n |\hat{x}^i - c_n^N| \quad (11)$$

$\{c_n^4\} = \{$	Ca _{0.23}	Sr _{0.27}	O _{0.50}
0.00	0.23	0.27	0.50
0.25	<u>0.02</u>	<u>0.02</u>	0.25
0.50	0.27	0.23	<u>0.00</u>
0.75	0.52	0.48	0.25
1.00	0.77	0.73	0.50
$\}$			

$$\text{Ca}_{0.23}\text{Sr}_{0.27}\text{O}_{0.50} (L_{\text{int}}^4 = 0.04)$$

$$\rightarrow \text{Ca}_{0.25}\text{Sr}_{0.25}\text{O}_{0.5}$$

$$\rightarrow \text{CaSrO}_2$$

Figure 2: An overview of the integer loss L_{int}^4 under the assumption that each unit cell contains four atoms. The numbers shown inside the dashed box represent all possible difference combinations between the integer-compatible set $\{c_n^4\}$ and the composition values. The total loss is obtained by selecting the minimum among these combinations for each element (indicated by the black underline) and summing them.

As an example, Fig. 2 shows the result of applying L_{int}^4 to $\text{Ca}_{0.23}\text{Sr}_{0.27}\text{O}_{0.50}$. We assume $N_{\text{unit}} = 4$ and guide the compositions toward the nearest values in $\{0.00, 0.25, 0.5, 0.75, 1.00\}$. Because it is difficult to fix N_{unit} in advance, we evaluate multiple candidates for N_{unit} and choose the one that yields the smallest loss. Concretely, we define L_{integer} as follows:

$$L_{\text{integer},\{N_{\text{unit}}\}}(\hat{x}) = \min_{N \in \{N_{\text{unit}}\}} L_{\text{int}}^N(\hat{x}). \quad (12)$$

This flexible approach selects a suitable integer grid even when the optimal cell size is unknown.

2.7 Optimisation procedure

KIAGO divides its optimisation into two stages. First, as in Section 2.3 and 2.4, we construct an initial \hat{x}_{base} and control which elements appear while iteratively minimising the following loss $L_{1\text{st}}$. This process yields $\hat{x}_{*}^{1\text{st}}$.

$$\hat{x} = x_{\text{const}} + \sigma(\hat{x}_{\text{base}} * M_{\text{elem}})(1 - \sum_i x_{\text{const}}^i) \quad (13)$$

$$L_{1\text{st}} = -f_{T_c}(\hat{x}) + \alpha f_{E_f}(\hat{x}) \quad (14)$$

$$\hat{x}_{*}^{1\text{st}} = \underset{\hat{x}_{\text{base}}}{\text{argmin}} L_{1\text{st}} \quad (15)$$

Next, we introduce the conversion to integers and a maximum-atom constraint. We use $\hat{x}_{*}^{1\text{st}}$ to build the mask $M_{\text{elem}}^{\text{max}}$, then iteratively minimise the loss $L_{2\text{nd}}$.

$$\hat{x}'(\hat{x}_{\text{base}}) = x_{\text{const}} +$$

$$\sigma(\hat{x}_{\text{base}} * M_{\text{elem}}^{\text{max}} * M_{\text{elem}})(1 - \sum_i x_{\text{const}}^i) \quad (16)$$

$$L_{2\text{nd}} = -f_{T_c}(\hat{x}') + \alpha f_{E_f}(\hat{x}') + \beta L_{\text{integer}, \{N_{\text{unit}}\}}(\hat{x}') \quad (17)$$

$$\hat{x}_*^{2\text{nd}} = \underset{\hat{x}_{\text{base}}}{\text{argmin}} L_{2\text{nd}} \quad (18)$$

Here, β is a hyperparameter. We take $\hat{x}'(\hat{x}_*^{2\text{nd}})$ as the final solution.

3 Results

3.1 Implementation Details

We used PyTorch [36] to implement KIAGO. KIAGO optimises a total of 4,096 candidate compositions across 1,000 steps using Adam optimiser [37]. We first perform 500 steps of optimisation using equations 13 to 15, followed by another 500 steps using equations 16 to 18 with $\alpha = 4$ (selected based on tuning) and $\beta = 1$. To predict the superconducting transition temperature (T_c), we employ a ResNet18 model [38] trained on normalised compositions of SuperCon and Crystallography Open Database (COD) [39, 40, 41, 42, 43, 44, 45, 46, 47]. Each composition is represented by a periodic table-based feature map, which has four channels corresponding to the s, p, d, and f orbitals [12]. For each element, we set flags at the positions of its row and column on the periodic table, as well as at its relevant orbital channels. We then multiply these element-level feature maps by the respective compositional ratios to create the final input representation. Further details are available in Section S.1. For formation energy, we used ElemNet [48], which is originally implemented in Tensorflow 1.x [49] and we re-implemented it in PyTorch. Since ElemNet only covers elements up to atomic number 86, we apply a mask to exclude elements beyond that range. Additional technical specifics are given in Section S.2.

We compared KIAGO against two baselines: a conventional elemental-substitution (C-ES) approach and SuperDiff, a diffusion-based generative model. The C-ES method randomly replaces some elements with others of identical oxidation states. For SuperDiff, we used the official implementation and train on the same data for our T_c prediction model, but without normalising compositions. Following the official code, we conducted 1,000 diffusion steps. According to the original SuperDiff, we conditioned generations of compositions on existing superconductors using Iterative Latent Variable Refinement (ILVR). We applied scale factors of 1, 2, 4, and 6 to yield a total of 4,096 samples. We also incorporate Classifier Guidance (CG) using T_c prediction model and ElemNet into SuperDiff to compare it directly with KIAGO. Normally, the classifier used for CG must be trained on data with noise, which would make Universal Guidance (UG) the better choice for off-the-shelf models. However, we found that UG did not work well and CG still improved T_c using models without noise-augmented training. Therefore, we decided to use CG. Although neither model is strictly a classifier, we refer to this approach as CG for convenience. Note that this

is not proposed in the original paper[24]. At each inference step, we used equation 14 with $\alpha = 4$ for gradient guidance, and we tune the guidance weight from 1×10^{-7} to 1.0, ultimately selecting 1×10^{-3} . Additional details of SuperDiff are provided in Section S.3.

After generating candidate compositions, we applied a multi-step screening procedure to ensure realistic materials. First, we used SMOG [50] to filter compositions with charge neutrality and electronegativity balance, following Yuan *et al.* [24]. Next, we selected only those with formation energies (predicted by ElemNet) less than zero. We also removed compositions containing ten or more elements since the preprocessed SuperCon data have at most nine. Finally, we evaluate T_c values using the same ResNet18 predictor used in KIAGO and SuperDiff with CG.

3.2 Mitigating the risk of convergence to non-promising solutions

In this section, we investigated whether our initialisation scheme could mitigate the risk of converging to non-promising local minima in the first stage (equations 13 to 15). Specifically, we aimed to determine whether our method can produce more promising local optima than a purely random initialisation. In our method, we began with the superconductor CuLa_2O_4 from the SuperCon dataset. With a probability of 0.22, we replaced elements of its composition with different elements chosen according to their occurrence frequencies in SuperCon. We then selected random elements with random compositional ratios (from 0.0 to 0.3) for those elements, normalised the resulting composition, and used it as the initialisation. By contrast, the random initialisation selects seven elements, to match the number of atoms in CuLa_2O_4 , uniformly at random and assigns them random compositional values.

Fig. 3 shows the optimisation results. Our initialisation scheme yields higher T_c values than random initialisation. Although our method can still become trapped in local optima, it proposes more promising solutions than the random approach. Hence, our approach partially mitigates the inherent challenge of local minima in gradient-based methods.

3.3 Converting compositional ratios to integers via loss-based approach

In this section, we compared integer conversion method based on a loss function $L_{\text{integer}, \{N_{\text{unit}}\}}$ with a rule-based integer conversion method. We aimed to determine which approach reduced the drop in T_c in the second stage (equations 16 to 18). In the loss-based method, we follow equation 17 to maximise T_c while minimising E_f . Specifically, we guided the composition toward an integer representation by selecting an optimal total number of atoms from a set of integers smaller than the specified maximum atom count. We optimised them for 500 steps for integer conversion. By contrast, the rule-based approach multiplies the

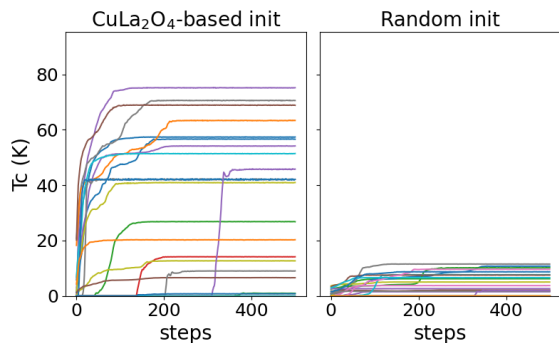


Figure 3: Comparison of optimisation results under different initialisation methods. Both approaches employ Adam optimiser [37] with a learning rate of 0.001. (Left) Initialisation by adding noise to an existing superconductor (CuLa_2O_4). (Right) Random initialisation, in which seven elements are chosen arbitrarily and assigned random compositional values.

Table 1: Comparison between the rule-based approach and $L_{integer, \{N_{unit}\}}$ for converting compositional ratios to integers. The table shows the average change in T_c before and after conversion to integers under certain maximum numbers of atoms, based on a total of 61,440 samples derived from 15 different superconducting materials.

Max Num Atoms	$L_{integer, \{N_{unit}\}}$ (K)	Rule-based (K)
15	-6.44	-8.22
20	-2.47	-3.27
25	-2.36	-3.40
50	-3.22	-1.13
100	-0.88	-0.27

normalised composition by the specified number of atoms and then rounds each value to the nearest integer.

Table 1 shows the results comparing the rule-based approach and $L_{integer, \{N_{unit}\}}$. Because it remains closer to the pre-conversion to integers composition, rounding with a larger total number of atoms is generally advantageous. Although the rule-based method fully exploits this by always rounding at the maximum atom count, $L_{integer, \{N_{unit}\}}$ does not always do so, yet it still often performs better.

3.4 Generating superconductors with higher T_c based on existing ones

In this section, we investigated whether our method could propose superconductors with higher T_c values based on known superconductors as initial candidates. For KIAGO, we start with existing superconductors and introduce noise to the compositions described in Section 3.2. We used Adam optimiser with learning rate of 0.03 for KIAGO. We set $\{N_{unit}\} = \{1, 2, \dots, 25\}$ and $n_{elem}^{max} = 25$. SuperDiff conditions on existing superconductors via Iterative Latent Variable Refinement (ILVR). The conventional elemental-substitution (C-ES) approach randomly replaces a sub-

Table 2: Differences in T_c (K) between the average T_c of the highest Top-30 proposed superconductors and the base superconductors in the experiments of proposing superconductors based on existing ones. SD, SD w/ CG, and C-ES denote SuperDiff, SuperDiff with Classifier Guidance, and conventional elemental substitution, respectively. After screening 4096 samples, the T_c prediction model was used to calculate T_c . 'N/A' indicates that none of the samples passed the screening.

Base materials from SuperCon	KIAGO Top-30 ΔT_c (K)	SD Top-30 ΔT_c (K)	SD w/ CG Top-30 ΔT_c (K)	C-ES Top-30 ΔT_c (K)
LaNiAsO	97.64	-1.42	-0.48	16.79
SrFe _{1.88} Ni _{0.12} As ₂	86.77	26.76	0.74	18.96
Sr ₄ V ₂ Fe ₂ As ₂ O ₆	89.89	-13.77	-3.99	0.00
LaPt ₂ B ₂ C	86.39	-5.01	-5.27	5.06
HgBa ₂ Ca ₂ Cu ₃ O ₈	16.70	-29.43	-21.36	1.00
CeBiS ₂ O	94.89	N/A	N/A	0.42
Bi ₂ Sr ₂ CuO ₆	127.33	18.34	14.38	52.25
TlSr ₂ CaCu ₂ O ₇	74.64	5.21	11.53	34.07

set of elements with others sharing the same oxidation state. For each base material of superconductor, we select copper-based, iron-based, and other superconductors that pass charge-neutrality and electronegativity screening by SMACT, then randomly choose from these sets as base materials.

Table 2 presents the differences in predicted T_c between the generated superconductors and their base materials. KIAGO achieves the most efficient exploration of higher T_c values compared to other methods. By contrast, there are experiments where SuperDiff does not yields any valid materials passing all screenings. This limitation may stem from the fact that many entries in SuperCon do not pass charge-neutrality and electronegativity checks; hence, the model struggles to generate valid compositions. The C-ES method also fails to propose sufficiently high T_c compounds, likely because its rule-based approach cannot fully explore the vast compositional space. In contrast, KIAGO proposes many materials showing substantial T_c increases. For completeness, Section S.5 includes all screening-pass rates.

Table 3 describes example compositions. Both KIAGO and C-ES yield integer-total compositions, allowing straightforward induction of possible crystal structures. However, SuperDiff and SuperDiff with CG frequently produce non-integer totals, making immediate structural analysis more challenging.

Interestingly, SuperDiff with CG does not necessarily generate higher- T_c compounds than SuperDiff alone. Table 4 shows how T_c changes in guidance and denoising under different weights for guidance. During generation, high guidance weights raise T_c in the guidance step but then revert it in the ILVR and denoising step. We attribute this to the T_c distribution in SuperCon, where low- or moderate- T_c compounds dominate (median: 12.5 K). As a result, extremely high T_c values are treated as noise, prompting the model to restore them to more typical levels. Furthermore,

Table 3: Samples of proposed superconductors.

Method	Samples
KIAGO	$\text{Be}_2\text{Ca}_3\text{Cu}_3\text{Ce}_2\text{HgO}_9$ (112.25K)
	$\text{MgCa}_3\text{Cu}_3\text{Ba}_3\text{BiO}_9$ (142.72K)
	$\text{Ca}_4\text{Cu}_5\text{Sr}_4\text{NdN}_2\text{As}_5$ (102.25K)
	$\text{Ca}_5\text{Cu}_4\text{Sr}_4\text{CO}_{10}$ (129.11K)
SD	$\text{Ni}_{0.99}\text{LaO}_{1.01}\text{AsO}_{0.99}$ (3.65K)
	$\text{Ni}_{0.82}\text{Ge}_{0.25}\text{La}_{0.97}\text{C}_{1.59}\text{As}_{0.44}\text{Se}_{0.14}$ (1.23K)
	$\text{Ca}_{0.28}\text{Cu}_{1.39}\text{Sr}_{2.04}\text{Pb}_{0.91}\text{Bi}_{1.15}\text{O}_{7.03}$ (76.03K)
	$\text{Ca}_{1.84}\text{Sc}_{0.17}\text{Cu}_{2.91}\text{Ba}_{2.05}\text{HgO}_{8.05}$ (127.46K)
SD w/ CG	$\text{Be}_{357.07}\text{Fe}_{0.31}\text{Co}_{0.21}\text{Zn}_{0.21}\text{Ge}_{0.93}\text{La}_{1.06}$ (8.41K)
	$\text{Ca}_{1.98}\text{Cu}_3\text{Ba}_{2.01}\text{HgN}_{0.2}\text{O}_{7.79}$ (125.64K)
	$\text{Ca}_{2.04}\text{Cu}_3\text{Ba}_{2.07}\text{Hg}_{1.09}\text{O}_{8.2}$ (126.48K)
	$\text{CaCu}_2\text{Sr}_{1.99}\text{Hg}_{0.77}\text{Bi}_{0.36}\text{O}_{7.03}$ (82.81K)
C-ES	$\text{Ca}_2\text{Cu}_6\text{Sr}_4\text{O}_{14}$ (103.89K)
	$\text{CaCu}_3\text{Sr}_2\text{O}_7$ (103.89K)
	$\text{Ga}_4\text{Ti}_6\text{Bi}_{18}\text{O}_{18}\text{Si}_8\text{S}_{36}$ (3.30K)
	$\text{Ca}_6\text{Cu}_{18}\text{Sr}_{12}\text{O}_{42}$ (103.89K)

Table 4: Total changes in T_c resulting from guidance, ILVR, and denoising during the 1000 steps in SuperDiff w/ CG. "Guide weight" denotes the weight for guidance. "Denoise ΔT_c ", "ILVR ΔT_c " and "Guide ΔT_c " represent the cumulative change in T_c per step due to denoising, ILVR, or the guidance. "Sum" is the total of these values. "Screening ratio" denotes the ratio of the number of screened samples to the total number of samples.

Guide weight w	Denoise ΔT_c (K)	ILVR ΔT_c (K)	Guide ΔT_c (K)	Sum (K)	Screening ratio
-	12.9	-3.4	-	9.5	0.08
1.0e-05	12.1	-2.5	0.0	9.5	0.08
1.0e-04	12.6	-2.6	0.0	10.0	0.08
1.0e-03	12.9	-3.7	0.3	9.5	0.08
1.0e-02	11.9	-4.9	2.6	9.7	0.09
1.0e-01	6.7	-22.0	25.3	9.9	0.08
1.0e+00	-33.4	-254.1	309.0	21.5	0.00
1.0e+01	-40.1	-1658.2	1774.3	76.0	0.00
1.0e+02	-18.2	-1075.8	1141.9	48.0	0.00

larger weight for guidance cause a stronger mismatch with the training distribution, reducing the fraction of generated compositions that contain fewer than ten elements. This interplay of denoising and guidance likely hampers SuperDiff with CG's ability to reach stable, high- T_c solutions. For the results without ILVR, please refer to Section S.3.

3.5 Elemental substitution

In this section, we implemented elemental substitution to improve T_c . Here we replaced one metal element based on its oxidation state while retaining the rest of the composition. Specifically, we chose a single metal element from an existing superconductor and kept the remaining composition fixed.

We implement this approach in KIAGO by treating the preserved composition as a fixed vector x_{const} . We then randomly initialise the substituting element and apply a mask based on its oxidation state. For example, when substituting Y^{+3} , we only allow elements having a +3 oxidation state, such as gallium or aluminum. To achieve

Table 5: Success rate of elemental substitution in proposed materials. We defined a successful elemental substitution as satisfying both of the following criteria: 1) the preserved composition remains within 1% of its original ratio, and 2) the total composition of the newly substituted element (or elements) stays within 1% of the original substituted metal's ratio.

Base materials from SuperCon	Substitute target	KIAGO	SD	SD w/ CG	C-ES
$\text{CeFeAsF}_{0.2}\text{O}_{0.8}$	Ce^{+3}	1.00	0.00	0.00	1.00
$\text{LaFeAsO}_{1.0}$	La^{+3}	1.00	0.01	0.01	1.00
SrFe_2As_2	Sr^{+2}	1.00	0.01	0.01	1.00
$\text{Bi}_2\text{CaSr}_2\text{Cu}_2\text{O}_8$	Bi^{+3}	1.00	0.23	0.22	1.00
CeNiC_2	Ce^{+4}	1.00	0.00	0.00	1.00
LaNiC_2	La^{+3}	1.00	0.01	0.01	1.00
MgCoNi_3	Co^{+2}	1.00	0.00	0.00	1.00
$\text{RuSr}_2\text{GdCu}_2\text{O}_8$	Sr^{+2}	1.00	0.03	0.03	1.00
$\text{RuSr}_2\text{YCu}_2\text{O}_8$	Y^{+3}	1.00	0.03	0.03	1.00
$\text{Y}_2\text{Fe}_3\text{Si}_5$	Y^{+3}	1.00	0.00	0.00	1.00
YIrSi	Y^{+3}	1.00	0.00	0.00	1.00

this, we used a mask that has one value on elements having a +3 oxidation state and set all others to zero. To simplify evaluation, we excluded the preserved elements from the mask. We use Adam optimiser with learning rate of 0.03 for KIAGO. Note that we did not perform conversion to integers on the substituting element, so we set $\beta = 0$. By contrast, SuperDiff does not explicitly support elemental substitution, so we approximated it by conditioning the generation process with ILVR.

In addition to the screening described in Section 3.1, we assessed whether the intended elemental substitution was correctly carried out. First, we checked whether the preserved composition remains within 1% of its original ratio. Second, we checked that the total composition of the newly substituted element (or elements) stays within 1% of the original substituted metal's ratio. To simplify evaluation, we excluded the preserved elements from the substituted element candidates. We then evaluated the T_c of compositions that pass both this substitution check and the previous screening.

Tables 5, 6, and 7 summarize the probability of correct element evaluation, the charge-neutrality evaluation, and the resulting T_c values, respectively. Notably, KIAGO and C-ES achieve 100% correct substitutions (Table 5), indicating that these methods incorporate domain knowledge effectively. Consequently, as shown in Table 6, their proposed materials always satisfy charge neutrality. Moreover, KIAGO demonstrates high search efficiency, yielding the best results in most experiments (Table 7). SuperDiff, however, cannot reliably perform elemental substitution, indicating that generative models like SuperDiff are not well suited when strict domain knowledge must be enforced.

Next, we compare the highest- T_c compounds in the SuperCon dataset that have undergone the same elemental substitution with the compounds proposed by KIAGO. Table 8 shows that, in most element-substitution experiments, KI-

Table 6: Success rate with respect to charge neutrality in proposed materials resulting from elemental substitution.

Base materials from SuperCon	Substitute target	KIAGO	SD	SD w/ CG	C-ES
CeFeAsF _{0.2} O _{0.8}	Ce ⁺³	1.00	0.03	0.02	1.00
LaFeAsO _{1.0}	La ⁺³	1.00	0.02	0.02	1.00
SrFe ₂ As ₂	Sr ⁺²	1.00	0.03	0.04	1.00
Bi ₂ CaSr ₂ Cu ₂ O ₈	Bi ⁺³	1.00	0.01	0.01	1.00
CeNiC ₂	Ce ⁺⁴	1.00	0.07	0.06	1.00
LaNiC ₂	La ⁺³	1.00	0.03	0.04	1.00
MgCoNi ₃	Co ⁺²	1.00	0.71	0.66	1.00
RuSr ₂ GdCu ₂ O ₈	Sr ⁺²	1.00	0.05	0.06	1.00
RuSr ₂ YC _u ₂ O ₈	Y ⁺³	1.00	0.08	0.07	1.00
Y ₂ Fe ₃ Si ₅	Y ⁺³	1.00	0.18	0.43	1.00
YIrSi	Y ⁺³	1.00	0.28	0.37	1.00

Table 7: Differences in T_c (K) between the average T_c of the highest Top-30 proposed superconductors and the base superconductors in experiments of elemental substitution. After screening 4096 samples, the T_c prediction model was used to calculate T_c . 'N/A' indicates that none of samples passed the screening.

Base materials from SuperCon	Substitute target	KIAGO Top-30 ΔT_c (K)	SD Top-30 ΔT_c (K)	SD w/ CG Top-30 ΔT_c (K)	C-ES Top-30 ΔT_c (K)
CeFeAsF _{0.2} O _{0.8}	Ce ⁺³	14.53	N/A	N/A	9.99
LaFeAsO _{1.0}	La ⁺³	35.62	1.24	N/A	29.45
SrFe ₂ As ₂	Sr ⁺²	29.35	N/A	N/A	13.78
Bi ₂ CaSr ₂ Cu ₂ O ₈	Bi ⁺³	14.61	0.15	-0.27	6.42
CeNiC ₂	Ce ⁺⁴	17.30	N/A	N/A	6.26
LaNiC ₂	La ⁺³	25.24	N/A	0.11	7.55
MgCoNi ₃	Co ⁺²	N/A	N/A	N/A	-2.41
RuSr ₂ GdCu ₂ O ₈	Sr ⁺²	-33.66	-0.23	0.93	3.70
RuSr ₂ YC _u ₂ O ₈	Y ⁺³	46.16	-0.89	-1.58	37.60
Y ₂ Fe ₃ Si ₅	Y ⁺³	7.56	N/A	N/A	1.45
YIrSi	Y ⁺³	5.08	3.42	N/A	5.31

AGO proposes materials with higher T_c than any element-substituted materials in the SuperCon dataset. This result highlights the potential of our approach to surpass known substitution strategies and discover more promising superconductors.

In this section, we limit our discussion to single-element substitution. However, our method can also support multi-element substitution. For example, in Ti₂O₄, two Ti⁴⁺ atoms and one O²⁻ atom contribute a total charge of +6. This can be replaced by two X³⁺ atoms, resulting in a composition like X₂O₃. Here, X denotes any element with a +3 oxidation state. Such substitutions are feasible as long as the total charge is preserved, and our oxidation-state-based masking mechanism can accommodate them.

3.6 Proposing novel hydride superconductors

In this section, we focused on proposing novel hydride superconductors (HSC). Many known HSC are binary or ternary systems containing hydrogen and just one or two other elements, with hydrogen comprising a large fraction of the composition. Thus, we constrained KI-

AGO to compositions that have at least 40% hydrogen to expand the space around existing materials, form binary or ternary compounds, and possess a total atom count of 15 or fewer. HSC are often tested under high pressure, where Pauling’s electronegativity rules may not hold. For instance, LaH₁₀ has been experimentally confirmed but fails SMACT-based screening for electronegativity and charge neutrality, because SMACT assumes each element has a single fixed valence. Then, we assumed each atom of the same element could adopt different valences. For example, hydrogen can be both +1 and -1, making LaH₁₀ = {La⁺², H⁻¹ × 6, H⁺¹ × 4}, which is thus electrically neutral. However, allowing multiple valences can lead to a combinatorial explosion, so we imposed a maximum total of 15 atoms per composition. We used these criteria (charge neutrality under variable valences, ternary or binary composition, and a total of 15 or fewer atoms) as a replacement for SMACT-based screening.

For initialisation for KIAGO, we began with HSC from the SuperCon dataset. With a probability of 0.29, we replaced elements of its composition with different elements chosen according to their occurrence frequencies in SuperCon. We then selected random elements with random compositional ratios (from 0.0 to 0.03) for those elements, normalised the resulting composition, and used it as the initialisation. We also set $\{N_{\text{unit}}\} = \{1, 2, \dots, 15\}$.

In Table 9, we present the average T_c of the top five proposed hydride superconductors. Compared with other methods, KIAGO efficiently generates hydride superconductors. Table 10 shows the probability of proposing materials that meet specific criteria—namely, having at least 40% hydrogen content, three or fewer elements, and a total atom count of 15 or below. These results indicate that KIAGO not only explores the search space efficiently but also strictly adheres to the specified constraints.

Table 11 lists HSC proposed by KIAGO. Notably, KIAGO also proposed materials made of the same elements as those in known compounds from the SuperCon dataset. In addition, it suggested materials that are not in SuperCon dataset but have been reported in other literature.

4 Limitation

Our method relies heavily on the accuracy of the prediction models. Although our current T_c predictor achieves competitive performance compared with other methods (see Section S.1.3), the predicted T_c values for the proposed materials inevitably contain some error. In addition, since the SuperCon dataset lacks pressure information—crucial for hydride superconductors—our model cannot address pressure effects, which could pose another limitation. Improving the prediction model’s accuracy must involve ensemble methods [14], better model architectures, or enhanced datasets. Importantly, our method does not depend on any specific model architecture. Given the rapid pace of machine-learning advances, more accurate models will likely become available soon, and substituting them into

Table 8: Comparison between materials proposed by KIAGO and the highest- T_c compounds from the SuperCon dataset under the same element-substitution conditions. All T_c values are prediction values by our T_c prediction model. Blue elements indicate the substituted elements.

Base materials from SuperCon	Substitute target	Proposed Samples	Best in SuperCon
CeFeAsF _{0.2} O _{0.8} (39.8 K)	Ce ⁺³	Ti _{0.1807} Sm _{0.8193} FeAsF _{0.2} O _{0.8} (57.08 K)	Gd FeAsF _{0.2} O _{0.8} (48.3 K)
LaFeAsO _{1.0} (13.4 K)	La ⁺³	Nd _{0.6077} Gd _{0.3239} Tb _{0.0684} FeAsO (53.64 K)	Sm _{0.65} Th _{0.35} FeAsO (52.9 K)
SrFe ₂ As ₂ (17.3 K)	Sr ⁺²	Mg _{0.2089} V _{0.0183} La _{0.243} Nd _{0.251} Eu _{0.2014} Dy _{0.0774} Fe ₂ As ₂ (47.59 K)	Ba _{0.66} K _{0.34} Fe ₂ As ₂ (38.6 K)
Bi ₂ CaSr ₂ Cu ₂ O ₈ (81.0 K)	Bi ⁺³	Hf _{0.2381} Pt _{0.5835} Bi _{1.1784} CaSr ₂ Cu ₂ O ₈ (95.88 K)	Bi _{1.2} Pb _{0.8} CaSr ₂ Cu ₂ O ₈ (92.9 K)
CeNiC ₂ (3.0 K)	Ce ⁺⁴	N _{0.1514} S _{0.1395} V _{0.086} Zr _{0.2171} Rh _{0.3626} Pr _{0.0434} NiC ₂ (20.91 K)	Th _{0.1} Y _{0.9} NiC ₂ (6.6 K)
LaNiC ₂ (2.4 K)	La ⁺³	Zr _{0.1793} Rh _{0.4886} Sb _{0.293} Pr _{0.0391} NiC ₂ (27.82 K)	Th _{0.1} Y _{0.9} NiC ₂ (6.6 K)
MgCoNi ₃ (7.4 K)	Co ⁺²	N/A	MgCuNi ₃ (7.6 K)
RuSr ₂ GdCu ₂ O ₈ (33.7 K)	Sr ⁺²	Ru N _{0.4994} Br _{0.5585} Nd _{0.5374} Er _{0.4047} GdCu ₂ O ₈ (0.00 K)	Ru Ba _{0.4} Sr _{1.6} GdCu ₂ O ₈ (40.7 K)
RuSr ₂ YCu ₂ O ₈ (34.4 K)	Y ⁺³	RuSr ₂ Ti _{0.3309} Nd _{0.1602} W _{0.2576} Bi _{0.2513} Cu ₂ O ₈ (80.61 K)	RuSr ₂ Ca _{0.1} Gd _{0.9} Cu ₂ O ₈ (60.4 K)
Y ₂ Fe ₃ Si ₅ (2.3 K)	Y ⁺³	Pr _{0.4884} Sm _{0.1106} Gd _{0.3835} Dy _{0.4279} Ho _{0.3464} Hf _{0.2432} Fe ₃ Si ₅ (9.90 K)	Lu ₂ Fe ₃ Si ₅ (5.3 K)
YIrSi (2.8 K)	Y ⁺³	Co _{0.1167} La _{0.0731} Ce _{0.1664} Sm _{0.2572} Eu _{0.2764} Tb _{0.1102} IrSi (10.15 K)	Th IrSi (6.9 K)

Table 9: Average T_c for the Top-5 proposed superconductors

Base materials from SuperCon	KIAGO Top-5 T_c (K)	SD Top-5 T_c (K)	SD w/ CG Top-5 T_c (K)	C-ES Top-5 T_c (K)
PdH	3.58	0.00	0.10	3.03
PtH	3.13	0.00	0.00	3.07
LaH ₁₀	3.72	0.00	0.00	0.00
H ₂ S	3.10	0.14	0.14	0.00
H ₄ Si	3.13	0.00	0.00	0.00

Table 10: Ratio of proposed materials satisfying the following three conditions: (1) Hydrogen(H) content is 40% or more, (2) composed of three or fewer elements, and (3) 15 atoms or less.

Base materials from SuperCon	KIAGO	SD	SD w/ CG	C-ES
PdH	1.00	0.03	0.02	1.00
PtH	1.00	0.03	0.03	1.00
LaH ₁₀	1.00	0.02	0.02	1.00
H ₂ S	1.00	0.04	0.03	1.00
H ₄ Si	1.00	0.03	0.02	1.00

Table 11: Candidates of hydride superconductor proposed by KIAGO. The 'Similar formula in Refs' and ' T_c in Refs' columns show the composition and T_c of superconductors experimentally confirmed or calculated by DFT in other studies, respectively, which are composed of the same elements as the proposed materials.

Proposed formula	Predicted T_c (K)	Similar formula in dataset	T_c (K) in SuperCon	Similar formula in Refs	T_c (K) in Refs
SiH	0.7	SiH ₄	17.0	-	-
ZrH	0.5	-	-	ZrH ₃	6.7 ^{EXP} [51]
H ₉ Mo ₅	6.7	-	-	MoH ₆	80 ^{DFT} [52]
Be ₂ H ₅	2.3	-	-	BeH ₃	181 ^{DFT} [53]
Bi ₇ H ₅	3.8	-	-	BiH ₄	91 ^{DFT} [54]
Ge ₇ H ₅	2.3	-	-	GeH ₄	64 ^{DFT} [55]

our framework should alleviate current limitations. Additionally, datasets are also improving at a fast rate, offering further opportunities for refinement.

Conclusion

In this paper, we introduced KIAGO, a gradient-based method for proposing high- T_c superconductors that unify domain knowledge with efficient computational strategies. Unlike Classifier Guidance-based generative models, KIAGO does not require to train additional generative models, making it a more straightforward solution. By initialising the optimisation from promising superconductors, we mitigate the risk of converging to poor local minima—an issue often encountered in gradient-based methods—and achieve higher optimisation efficiency. A key strength of KIAGO lies in its ability to incorporate diverse domain knowledge via masking. We demonstrated this by precisely controlling elemental substitutions and restricting our search to hydride superconductors. These results underscore the adaptability of KIAGO: it not only capitalizes on existing knowledge, like traditional doping strategies but also explores a broader chemical space more effectively than previous approaches. Overall, KIAGO paves the way for discovering new materials by exploiting domain knowledge and machine learning’s scalability. This synergy has the potential to accelerate advancements in high- T_c superconductivity and beyond, offering a robust framework for rapid and adaptive materials design.

Conflicts of interest

There are no conflicts to declare.

Acknowledgement

The authors gratefully acknowledge support from the Doctoral Student Special Incentives Program, Graduate School of Engineering, The University of Tokyo (SEUT-RA).

Data availability

The code used to implement the optimization framework in this study is available at Zenodo: <https://doi.org/10.5281/zenodo.15477853>, which archives the GitHub repository at <https://github.com/AkiraT0SEI/KIAG0>. This version corresponds to the release v0.1.0, accessed on 20 May 2025. Trained models for the T_c predictor and formation energy predictor are also provided in this repository. The SuperCon dataset is available at <https://mdr.nims.go.jp/collections/5712mb227>. The ElemNet training data can be obtained from <http://cucis.ece.northwestern.edu/projects/DataSets/ElemNet/data.tar.gz>, and the COD database can be accessed at <https://www.crystallography.net/cod/>.

References

- [1] John R Hull. Applications of high-temperature superconductors in power technology. *Reports on Progress in Physics*, 66(11):1865, 2003.
- [2] Davide Uglietti. A review of commercial high temperature superconducting materials for large magnets: from wires and tapes to cables and conductors. *Superconductor Science and Technology*, 32(5):053001, 2019.
- [3] JMS Skakle. Crystal chemical substitutions and doping of $\text{YBa}_2\text{Cu}_3\text{O}_x$ and related superconductors. *Materials Science and Engineering: R: Reports*, 23(1):1–40, 1998.
- [4] YY Yao, CH Song, P Bao, D Su, XM Lu, JS Zhu, and YN Wang. Doping effect on the dielectric property in bismuth titanate. *Journal of Applied Physics*, 95(6):3126–3130, 2004.
- [5] Steven C Erwin, Lijun Zu, Michael I Haftel, Alexander L Efros, Thomas A Kennedy, and David J Norris. Doping semiconductor nanocrystals. *Nature*, 436(7047):91–94, 2005.
- [6] R Terzioglu, G Aydin, N Soylu Koc, and C Terzioglu. Investigation of the structural, magnetic and electrical properties of the Au doped YBCO superconductors. *Journal of Materials Science: Materials in Electronics*, 30:2265–2277, 2019.
- [7] Valentin Stanev, Corey Osos, A Gilad Kusne, Efrain Rodriguez, Johnpierre Paglione, Stefano Curtarolo, and Ichiro Takeuchi. Machine learning modeling of superconducting critical temperature. *npj Computational Materials*, 4(1):29, 2018.
- [8] Kaname Matsumoto and Tomoya Horide. An acceleration search method of higher T_c superconductors by a machine learning algorithm. *Applied Physics Express*, 12(7):073003, 2019.
- [9] Shuming Zeng, Yinchang Zhao, Geng Li, Ruirui Wang, Xinming Wang, and Jun Ni. Atom table convolutional neural networks for an accurate prediction of compounds properties. *NPJ Computational Materials*, 5(1):84, 2019.
- [10] Yabo Dan, Rongzhi Dong, Zhuo Cao, Xiang Li, Chengcheng Niu, Shaobo Li, and Jianjun Hu. Computational prediction of critical temperatures of superconductors based on convolutional gradient boosting decision trees. *IEEE Access*, 8:57868–57878, 2020.
- [11] Thanh Dung Le, Rita Noumeir, Huu Luong Quach, Ji Hyung Kim, Jung Ho Kim, and Ho Min Kim. Critical temperature prediction for a superconductor: A variational bayesian neural network approach. *IEEE Transactions on Applied Superconductivity*, 30(4):1–5, 2020.
- [12] Tomohiko Konno, Hodaka Kurokawa, Fuyuki Nabeshima, Yuki Sakishita, Ryo Ogawa, Iwao Hosako, and Atsutaka Maeda. Deep learning model for finding new superconductors. *Physical Review B*, 103(1):014509, 2021.
- [13] Jingzi Zhang, Zhuoxuan Zhu, X-D Xiang, Ke Zhang, Shangchao Huang, Chengquan Zhong, Hua-Jun Qiu, Kailong Hu, and Xi Lin. Machine learning prediction of superconducting critical temperature through the structural descriptor. *The Journal of Physical Chemistry C*, 126(20):8922–8927, 2022.
- [14] AmirMasoud Taheri, Hossein Ebrahimnezhad, and Mohammad Hossein Sedaaghi. Prediction of the critical temperature of superconducting materials using image regression and ensemble deep learning. *Materials Today Communications*, 33:104743, 2022.
- [15] Jingzi Zhang, Ke Zhang, Shaomeng Xu, Yi Li, Chengquan Zhong, Mengkun Zhao, Hua-Jun Qiu, Mingyang Qin, X-D Xiang, Kailong Hu, et al. An integrated machine learning model for accurate and robust prediction of superconducting critical temperature. *Journal of Energy Chemistry*, 78:232–239, 2023.
- [16] National Institute for Materials Science. Supercon.
- [17] Tian Xie, Xiang Fu, Octavian-Eugen Ganea, Regina Barzilay, and Tommi Jaakkola. Crystal diffusion variational autoencoder for periodic material generation. *arXiv preprint arXiv:2110.06197*, 2021.
- [18] Zekun Ren, Siyu Isaac Parker Tian, Juhwan Noh, Felipe Oviedo, Guangzong Xing, Jiali Li, Qiaohao Liang, Ruiming Zhu, Armin G Aberle, Shijing Sun, et al. An invertible crystallographic representation for general inverse design of inorganic crystals with targeted properties. *Matter*, 5(1):314–335, 2022.
- [19] Claudio Zeni, Robert Pinsler, Daniel Zügner, Andrew Fowler, Matthew Horton, Xiang Fu, Sasha Shysheya, Jonathan Crabbé, Lixin Sun, Jake Smith, et al. Mat-tergen: a generative model for inorganic materials design. *arXiv preprint arXiv:2312.03687*, 2023.

- [20] Zhenze Yang, Weike Ye, Xiangyun Lei, Daniel Schweigert, Ha-Kyung Kwon, and Arash Khajeh. De novo design of polymer electrolytes using gpt-based and diffusion-based generative models. *npj Computational Materials*, 10(1):296, 2024.
- [21] Chengquan Zhong, Jingzi Zhang, Xiaoting Lu, Ke Zhang, Jiakai Liu, Kailong Hu, Junjie Chen, and Xi Lin. Deep generative model for inverse design of high-temperature superconductor compositions with predicted $T_c > 77$ K. *ACS Applied Materials & Interfaces*, 15(25):30029–30038, 2023.
- [22] Evan Kim and SV Dordevic. Scgan: A generative adversarial network to predict hypothetical superconductors. *Journal of Physics: Condensed Matter*, 36(2):025702, 2023.
- [23] Daniel Wines, Tian Xie, and Kamal Choudhary. Inverse design of next-generation superconductors using data-driven deep generative models. *The Journal of Physical Chemistry Letters*, 14(29):6630–6638, 2023.
- [24] Samuel Yuan and SV Dordevic. Diffusion models for conditional generation of hypothetical new families of superconductors. *Scientific Reports*, 14(1):10275, 2024.
- [25] Jonathan Ho, Ajay Jain, and Pieter Abbeel. Denoising diffusion probabilistic models. *Advances in neural information processing systems*, 33:6840–6851, 2020.
- [26] Florinel-Alin Croitoru, Vlad Hondru, Radu Tudor Ionescu, and Mubarak Shah. Diffusion models in vision: A survey. *IEEE Transactions on Pattern Analysis and Machine Intelligence*, 45(9):10850–10869, 2023.
- [27] Jooyoung Choi, Sungwon Kim, Yonghyun Jeong, Youngjune Gwon, and Sungroh Yoon. Ilvr: Conditioning method for denoising diffusion probabilistic models. *arXiv preprint arXiv:2108.02938*, 2021.
- [28] Andrew Brock, Jeff Donahue, and Karen Simonyan. Large scale gan training for high fidelity natural image synthesis. *arXiv preprint arXiv:1809.11096*, 2018.
- [29] Arpit Bansal, Hong-Min Chu, Avi Schwarzschild, Soumyadip Sengupta, Micah Goldblum, Jonas Geiping, and Tom Goldstein. Universal guidance for diffusion models. In *Proceedings of the IEEE/CVF Conference on Computer Vision and Pattern Recognition (CVPR) Workshops*, pages 843–852, June 2023.
- [30] Prafulla Dhariwal and Alexander Nichol. Diffusion models beat gans on image synthesis. *Advances in neural information processing systems*, 34:8780–8794, 2021.
- [31] Jonathan Ho and Tim Salimans. Classifier-free diffusion guidance. *arXiv preprint arXiv:2207.12598*, 2022.
- [32] Simiao Ren, Willie Padilla, and Jordan Malof. Benchmarking deep inverse models over time, and the neural-adjoint method. *Advances in Neural Information Processing Systems*, 33:38–48, 2020.
- [33] Kelsey R Allen, Tatiana Lopez-Guevara, Kimberly Stachenfeld, Alvaro Sanchez-Gonzalez, Peter Battaglia, Jessica Hamrick, and Tobias Pfaff. Physical design using differentiable learned simulators. *arXiv preprint arXiv:2202.00728*, 2022.
- [34] Rakhoon Hwang, Jae Yong Lee, Jin Young Shin, and Hyung Ju Hwang. Solving pde-constrained control problems using operator learning. In *Proceedings of the AAAI Conference on Artificial Intelligence*, volume 36, pages 4504–4512, 2022.
- [35] Akihiro Fujii, Hideki Tsunashima, Yoshihiro Fukuhara, Koji Shimizu, and Satoshi Watanabe. Enhancing inverse problem solutions with accurate surrogate simulators and promising candidates. *arXiv preprint arXiv:2304.13860*, 2023.
- [36] Adam Paszke, Sam Gross, Soumith Chintala, Gregory Chanan, Edward Yang, Zachary DeVito, Zeming Lin, Alban Desmaison, Luca Antiga, and Adam Lerer. Automatic differentiation in pytorch. 2017.
- [37] Diederik P Kingma and Jimmy Ba. Adam: A method for stochastic optimization. *arXiv preprint arXiv:1412.6980*, 2014.
- [38] Kaiming He, Xiangyu Zhang, Shaoqing Ren, and Jian Sun. Deep residual learning for image recognition. In *Proceedings of the IEEE conference on computer vision and pattern recognition*, pages 770–778, 2016.
- [39] Antanas Vaitkus, Andrius Merkys, Thomas Sander, Miguel Quirós, Paul A Thiessen, Evan E Bolton, and Saulius Gražulis. A workflow for deriving chemical entities from crystallographic data and its application to the crystallography open database. *Journal of Cheminformatics*, 15(1):123, 2023.
- [40] Andrius Merkys, Antanas Vaitkus, Algirdas Grybauskas, Aleksandras Kononov, Miguel Quirós, and Saulius Gražulis. Graph isomorphism-based algorithm for cross-checking chemical and crystallographic descriptions. *Journal of cheminformatics*, 15(1):25, 2023.
- [41] Antanas Vaitkus, Andrius Merkys, and Saulius Gražulis. Validation of the crystallography open database using the crystallographic information framework. *Applied Crystallography*, 54(2):661–672, 2021.
- [42] Miguel Quirós, Saulius Gražulis, Saulė Girdziuskauskaitė, Andrius Merkys, and Antanas Vaitkus. Using smiles strings for the description of chemical connectivity in the crystallography open database. *Journal of cheminformatics*, 10(1):23, 2018.
- [43] Andrius Merkys, Antanas Vaitkus, Justas Butkus, Mykolas Okulič-Kazarinas, Visvaldas Kairys, and Saulius Gražulis. Cod::Cif::Parser: an error-correcting cif parser for the perl language. *Applied Crystallography*, 49(1):292–301, 2016.

- [44] Saulius Gražulis, Andrius Merkys, Antanas Vaitkus, and Mykolas Okulič-Kazarinas. Computing stoichiometric molecular composition from crystal structures. *Applied Crystallography*, 48(1):85–91, 2015.
- [45] Saulius Gražulis, Adriana Daškevič, Andrius Merkys, Daniel Chateigner, Luca Lutterotti, Miguel Quiros, Nadezhda R Serebryanaya, Peter Moeck, Robert T Downs, and Armel Le Bail. Crystallography open database (cod): an open-access collection of crystal structures and platform for world-wide collaboration. *Nucleic acids research*, 40(D1):D420–D427, 2012.
- [46] Saulius Gražulis, Daniel Chateigner, Robert T Downs, AFT Yokochi, Miguel Quirós, Luca Lutterotti, Elena Manakova, Justas Butkus, Peter Moeck, and Armel Le Bail. Crystallography open database—an open-access collection of crystal structures. *Applied Crystallography*, 42(4):726–729, 2009.
- [47] Robert T Downs and Michelle Hall-Wallace. The american mineralogist crystal structure database. *American mineralogist*, 88(1):247–250, 2003.
- [48] Dipendra Jha, Logan Ward, Arindam Paul, Wei-keng Liao, Alok Choudhary, Chris Wolverton, and Ankit Agrawal. Elemnet: Deep learning the chemistry of materials from only elemental composition. *Scientific reports*, 8(1):17593, 2018.
- [49] Martín Abadi, Ashish Agarwal, Paul Barham, Eugene Brevdo, Zhifeng Chen, Craig Citro, Greg S. Corrado, Andy Davis, Jeffrey Dean, Matthieu Devin, Sanjay Ghemawat, Ian Goodfellow, Andrew Harp, Geoffrey Irving, Michael Isard, Yangqing Jia, Rafal Jozefowicz, Lukasz Kaiser, Manjunath Kudlur, Josh Levenberg, Dandelion Mané, Rajat Monga, Sherry Moore, Derek Murray, Chris Olah, Mike Schuster, Jonathon Shlens, Benoit Steiner, Ilya Sutskever, Kunal Talwar, Paul Tucker, Vincent Vanhoucke, Vijay Vasudevan, Fernanda Viégas, Oriol Vinyals, Pete Warden, Martin Wattenberg, Martin Wicke, Yuan Yu, and Xiaoqiang Zheng. TensorFlow: Large-scale machine learning on heterogeneous systems, 2015. Software available from tensorflow.org.
- [50] Daniel W Davies, Keith T Butler, Adam J Jackson, Jonathan M Skelton, Kazuki Morita, and Aron Walsh. Smact: Semiconducting materials by analogy and chemical theory. *Journal of Open Source Software*, 4(38):1361, 2019.
- [51] Hui Xie, Wenting Zhang, Defang Duan, Xiaoli Huang, Yanping Huang, Hao Song, Xiaolei Feng, Yansun Yao, Chris J Pickard, and Tian Cui. Superconducting zirconium polyhydrides at moderate pressures. *The Journal of Physical Chemistry Letters*, 11(3):646–651, 2020.
- [52] Zhiguang Liao, Changdong Liu, Yue Zhang, Yongliang Guo, and Xuezhi Ke. First-principles study on crystal structures and superconductivity of molybdenum hydrides under high pressure. *Journal of Applied Physics*, 128(10):105901, 09 2020.
- [53] Kun Gao, Wenwen Cui, Jingming Shi, Artur P Durajski, Jian Hao, Silvana Botti, Miguel AL Marques, and Yinwei Li. Prediction of high-t c superconductivity in ternary actinium beryllium hydrides at low pressure. *Physical Review B*, 109(1):014501, 2024.
- [54] Pengfei Shan, Liang Ma, Xin Yang, Mei Li, Ziyi Liu, Jun Hou, Sheng Jiang, LiLi Zhang, Lifen Shi, Pengtao Yang, et al. Molecular hydride superconductor bih4 with t c up to 91 k at 170 gpa. *Journal of the American Chemical Society*, 147(5):4375–4381, 2024.
- [55] Guoying Gao, Artem R Oganov, Aitor Bergara, Miguel Martinez-Canales, Tian Cui, Toshiaki Iitaka, Yanming Ma, and Guangtian Zou. Superconducting high pressure phase of germane. *Physical review letters*, 101(10):107002, 2008.

S.1 T_c prediction model

We trained a deep learning model f_{T_c} to predict the critical temperature (T_c) from composition, utilizing the SuperCon dataset as the source of superconductor data. Konno *et al.* [12] reported that training only on the SuperCon dataset increases false positives (i.e., mistakenly predicting non-superconductors as superconductors), so we added the Crystallography Open Database (COD) [39, 40, 41, 42, 43, 44, 45, 46, 47] as a dataset of non-superconductors to training data. We trained the ResNet18 regression model using Adam optimiser [37] with a learning rate of 0.0001 and a batch size of 1024. Given that $T_c \geq 0$, we employed the Rectified Linear Unit (ReLU) as the activation function at the output layer.

S.1.1 Dataset

We used the SuperCon dataset for superconductor materials. For preprocessing, we excluded substances whose compositions were not quantitatively specified, such as those denoted by variables (e.g., x, y, z). We also used the Crystallography Open Database (COD) for the non-superconductor materials. Furthermore, compositions identical to those in the SuperCon data were excluded from the COD data.

For both SuperCon and COD, compositions were represented by 118-dimensional (from H to Og) distribution vectors x , normalised to sum to 1. The critical temperature (T_c) was used as the target variable y , setting $y=0$ for non-superconducting materials from the COD dataset and using the actual T_c values from the SuperCon dataset. For substances with identical compositional ratios but different T_c values, we calculated the mean T_c value. Consequently, we obtained 14,410 data points for the SuperCon dataset and 373,901 data points for the COD dataset. Materials with the same combination of elements may cause data leakage if they are split across different data partitions. Therefore, we ensured that materials with the same combination of elements were placed in the same data partition during the data split. We then randomly split these into training, validation, and test sets in the ratios of 0.80:0.05:0.15, respectively.

However, we were concerned about the model’s accuracy due to an imbalance in the training data resulting from a smaller number of superconductors compared to non-superconductors. Therefore, to address this imbalance, we augmented the training data by increasing the number of instances from the SuperCon dataset by a factor of 25 through replication.

S.1.2 Element representation

As element features \mathbf{a} , we utilized flag representations for the s, p, d, and f electron orbitals as embedded in the periodic table [12]. Each element i has a feature tensor \mathbf{a} with dimensions of $4 \times 7 \times 32$, representing the channels for the s, p, d, and f electron orbitals, periods, and groups. Note that, due to the extension of lanthanides and actinides in the group direction, the third dimension (group) extends to

32, not 18. For any element i , its feature \mathbf{a}^i assigns a value of 1 at the position in the periodic table corresponding to the outermost electron’s channel and 0 values for all other positions.

$$\mathbf{A}_i = \mathbf{a}^i, \quad (\text{S.1.1})$$

$$\mathbf{A} \in \{0, 1\}^{118 \times 4 \times 7 \times 32}, \quad (\text{S.1.2})$$

$$i \in \{\mathbf{H}, \mathbf{He}, \dots, \mathbf{Og}\} \quad (\text{S.1.3})$$

$$(\text{S.1.4})$$

$$\mathbf{A}_{ijkl} = \begin{cases} 1 & \text{if atom } i \text{ has its outermost electrons} \\ & \text{, family (group), and period} \\ & \text{corresponding to } j, k, \text{ and } l. \\ 0 & \text{otherwise} \end{cases} \quad (\text{S.1.5})$$

For instance, the hydrogen atom, which has a 1s electron in its outermost shell and belongs to the first period and group, is represented by the feature $\mathbf{a}^{\mathbf{H}}$. This feature has a value of one at position (1, 1, 1) and zeroes elsewhere. Similarly, the feature for chlorine, $\mathbf{a}^{\mathbf{Cl}}$, which contains 3p electrons in its outer shell and is located in the third period and seventeenth group, has a value of 1 at position (2, 3, 31) and zeros elsewhere. Fig. S.1.1 illustrates the corresponding channel of the outermost electron for each element. The composition’s representation is calculated by computing the product of the composition vector and the element features \mathbf{a} , as shown in Fig. S.1.2.

S.1.3 Prediction scores

Since previous methods were evaluated only on SuperCon data, we first evaluated our model solely on the SuperCon dataset (Table S.1.1). Note that it is not a direct comparison due to differences in dataset dividing. The previous studies did not describe whether they consider the combination of elements in the data split. We assume that the previous studies did not perform such data splitting. Our model was the only one trained on both SuperCon and COD datasets. Our model demonstrated competitive results compared to other methods when using only SuperCon data. The model trained using COD and considering the combination of elements in the data split scored worse than the model trained only on SuperCon. However, as we will discuss in Section S.1.4, it was found that using COD is important to reduce false positives. Therefore, we adopted this model.

Table S.1.1: Results on SuperCon data and comparison with other methods.

Method	Train Dataset	Elem Div	MAE	R2
Stanev <i>et al.</i> [7]	SuperCon	False?	-	0.88
Zeng <i>et al.</i> [9]	SuperCon	False?	4.21	0.97
Dan <i>et al.</i> [10]	SuperCon	False?	-	0.907
Taheri <i>et al.</i> [14]	SuperCon	False?	-	0.927
Ours	SuperCon	False	4.90	0.92
Ours	SuperCon + COD	True	7.84	0.80

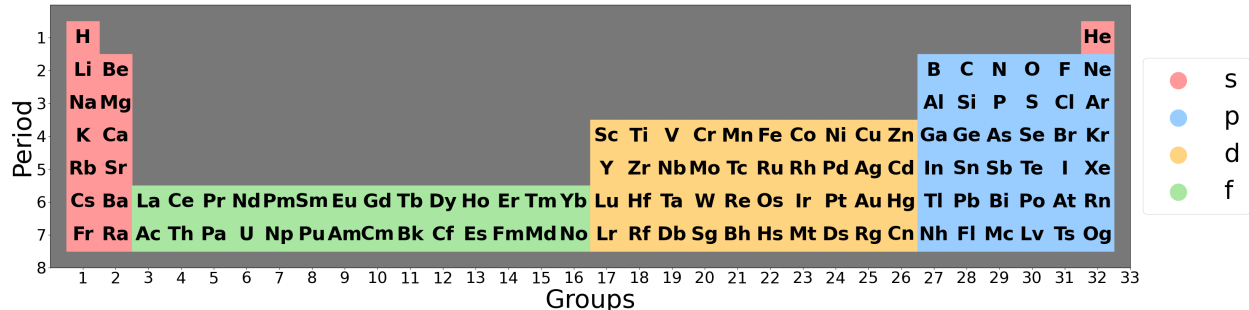


Figure S.1.1: Periodic table, coloured according to the type of orbital occupied by the outermost electron.

Table S.1.2: Precision scores with respect to the training set.

Training data	Precision score
SuperCon	0.065
SuperCon+COD	0.804

Table S.2.1: Comparison of MAE score of ElemNet with the original paper.

Methods	Original [48]	Our replication
MAE (eV/atom)	0.05	0.07

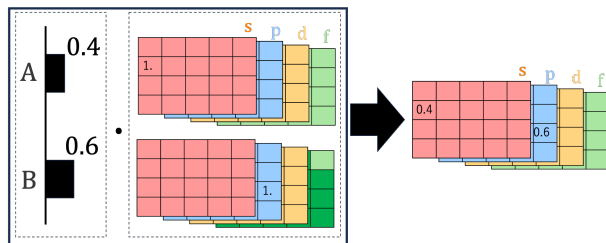


Figure S.1.2: Example: Representation of the composition A_2B_3

S.1.4 Reducing false positives

Here, we addressed the issue of false positives, that is, non-superconductors incorrectly predicted to be superconductors. Konno *et al.* [12] stated that models trained exclusively on the SuperCon dataset tend to produce a significant number of false positives, although this claim has not been numerically demonstrated. Hence, we numerically assessed how incorporating the COD dataset, which consists of non-superconductors, impacts the rate of false positives.

We performed this assessment using our model, a ResNet18 regression model and adopted the precision score as our metric. The precision score is defined as $tp/(tp + fp)$, where tp (true positive) denotes the probability of accurately predicting a superconductor ($y > 0$) as superconductor (i.e., $f_{T_c}(x) > 0$), and fp (false pos-

itive) represents the probability of mistakenly predicting a non-superconductor ($y=0$) as a superconductor (i.e., $f_{T_c}(x) > 0$).

Table S.1.2 provides a comparison of precision scores between models trained on the SuperCon dataset alone and those trained on both SuperCon and COD datasets. It is evident that models trained with the inclusion of the COD dataset exhibit a significantly higher precision score compared to those trained exclusively on the SuperCon dataset. This outcome underscores the necessity of integrating non-superconductors into the training process for superconductor material design tasks, where non-superconductors might emerge as potential candidates.

S.2 Formation energy prediction model

In this study, we employed ElemNet [48] as the formation energy prediction model. Although its original implementation (<https://github.com/NU-CUCIS/ElemNet>) use TensorFlow 1.x, we require gradient information in PyTorch. Thus, we re-implemented the model in PyTorch. We follow the same model architecture, training parameters, and dataset usage detailed in Jha *et al.* [48], and the performance of our re-implementation is presented in Table S.2.1.

S.3 SuperDiff and SuperDiff w/ CG

We implemented SuperDiff by following the procedures outlined in its original paper and official implementations. Specifically, we divided the dataset used for training the T_c prediction model into cuprates, pnictides, and others, then trained SuperDiff separately for each category. While the T_c prediction model was trained on normalised compositions, SuperDiff was trained without normalisation.

For conditional inference using Iterative Latent Variable Refinement (ILVR), we selected the appropriate SuperDiff model (cuprates, pnictides, or others) based on the reference material. We then applied guidance through ‘‘Classifier Guidance (CG)’’ using both the T_c prediction model and ElemNet with the loss function described in equation 1.

Table S.3.1: Total changes in T_c resulting from guidance and denoising during the 1000 steps in SuperDiff w/ CG **without ILVR**. "Guide weight" denotes the weight w used for guidance in Algorithm 2. "Denoise ΔT_c ", "ILVR ΔT_c " and "Guide ΔT_c " represent the cumulative change in T_c per step due to denoising, ILVR, or the guidance. "Sum" is the total of these values. "Screening ratio" denotes the ratio of the number of screened samples to the total number of samples.

Guide weight w	Denoise $\Delta T_c(K)$	ILVR $\Delta T_c(K)$	Guide $\Delta T_c(K)$	Sum (K)
-	20.0	-	-	20.0
1.0e-06	22.6	-	0.1	22.7
1.0e-05	20.1	-	0.6	20.6
1.0e-04	14.0	-	5.9	19.9
1.0e-03	-46.5	-	72.7	26.2
1.0e-02	-491.8	-	545.8	54.0
1.0e-01	-741.6	-	797.0	55.3
1.0e+00	-10.5	-	33.0	22.5

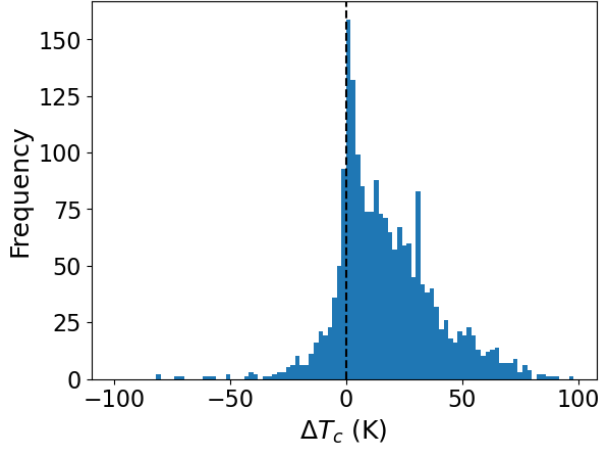


Figure S.4.1: Changes in T_c due to optimisation.

Although neither is strictly a classifier, we refer to this approach as CG for convenience. We describe two inference algorithms: one that performs ILVR-based conditional inference with SuperDiff in Algorithm 1, and one that further incorporates the two prediction models as guidance in Algorithm 2. Note that Algorithm 2 is not proposed in Yuan *et al.* [24].

Normally, the classifier used for CG must be trained on data with added noise, which would make Universal Guidance (UG) the better choice for off-the-shelf models. However, our experiments showed that CG still improved T_c without noise-augmented training. Therefore, we decided to use CG. We hypothesize that the reason CG remained effective despite the absence of noise-augmented training is that our T_c prediction model and formation energy prediction model both take normalised compositions as inputs, thereby reducing the impact of noise.

Algorithm 1 SuperDiff using ILVR Sampling Procedures

```

1:  $x_T \sim \mathcal{N}(\mathbf{0}, \mathbf{I})$ 
2: for  $t = T, \dots, 1$  do
3:    $z \sim \mathcal{N}(\mathbf{0}, \mathbf{I})$  if  $t > 1$ , else  $z = 0$ 
4:    $x'_{t-1} = \frac{1}{\sqrt{\alpha_t}} \left( x_t - \frac{1-\alpha_t}{\sqrt{1-\alpha_t}} \epsilon_\theta(x_t, t) \right) + \sigma_t z$   $\triangleright$ 
     Denoising
5:    $x_{t-1} = \phi_N(y_{t-1}) + x'_{t-1} - \phi_N(x'_{t-1})$   $\triangleright$  ILVR
     using sample  $y$ 
6: end for
7: return  $x_0$   $\triangleright$  Generated sample

```

Algorithm 2 SuperDiff using ILVR Sampling Procedures with Classifier Guidance

```

1:  $x_T \sim \mathcal{N}(\mathbf{0}, \mathbf{I})$ 
2: for  $t = T, \dots, 1$  do
3:    $z \sim \mathcal{N}(\mathbf{0}, \mathbf{I})$  if  $t > 1$ , else  $z = 0$ 
4:    $x'_{t-1} \leftarrow \frac{1}{\sqrt{\alpha_t}} \left( x_t - \frac{1-\alpha_t}{\sqrt{1-\alpha_t}} \epsilon_\theta(x_t, t) \right) + \sigma_t z$   $\triangleright$ 
     Denoising
5:    $x_{t-1} \leftarrow x_{t-1} - w \nabla L(x_{t-1})$   $\triangleright$  Guidance with
     predictors
6:    $x_{t-1} \leftarrow \phi_N(y_{t-1}) + x'_{t-1} - \phi_N(x'_{t-1})$   $\triangleright$  ILVR
     using sample  $y$ 
7: end for
8: return  $x_0$   $\triangleright$  Generated sample

```

S.3.1 Guidance vs denoise without ILVR

We also repeated the experiments from Table 4 without using ILVR. As shown in Table S.3.1, even without ILVR, excessive increases in T_c are still suppressed by denoising. We hypothesize that properties far from the data distribution are treated as "noise" by the diffusion model and consequently removed.

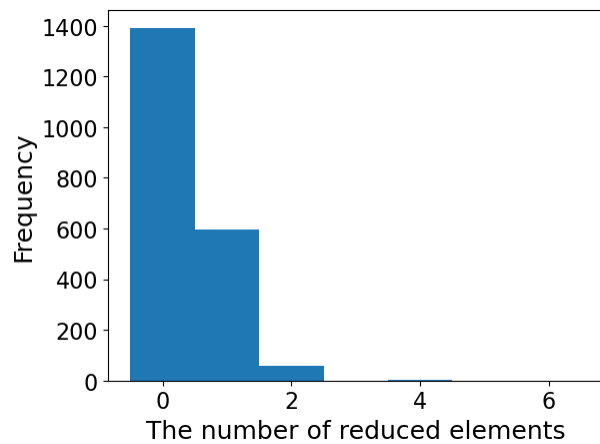
S.4 KIAGO optimisation in the first stage

Here, we show the results of the optimisation using equations 13 to 15. Fig. S.4.1 shows that most of samples have higher T_c after optimisation. However, some samples have lower T_c after optimisation. This is likely due to the presence of many local minima. Furthermore, we observed a tendency for the number of element types to decrease due to optimisation (Fig. S.4.2).

S.5 Detailed results

Table S.5.1 shows the detailed results of the experiments presented in Table 2 in Section 3.4. Each column in Table S.5.1 represents the fraction that fulfills each screening criterion. The last column shows the difference between the average T_c of the top 30 screened samples and the base materials.

Table S.5.2 shows the detailed results of the experiments presented in Table 5,6 and 7 in Section 3.5. Each col-



umn in Table S.5.2 represents the fraction that fulfills each screening criterion. The last column shows the difference between the average T_c of the top 30 screened samples and the base materials.

Figure S.4.2: Change in number of element types due to optimisation (a positive number denotes the number of element type decreases after optimisation).

Table S.5.1: All results of Screening rates and T_c . “Unique rate” indicates the fraction of unique compositions among the 4,096 samples. “ELM < 10,” “Neutrality,” “ElecNeg,” and “ $E_f < 0.0$ eV” denote, respectively, the percentage of these unique samples that: contain at most 9 elements (“ELM < 10”); satisfy charge neutrality per SMACT (“Neutrality”); meet electronegativity criterion using SMACT (“ElecNeg”); achieve predicted formation energy below 0.0 eV ($E_f < 0.0$ eV). “Screened rate” is the fraction that fulfills all these screening criteria among all 4,096 samples. “ ΔT_c Top-30 (K)” represents the difference between the average predicted T_c of the top 30 screened samples and the base materials.

Base materials from SuperCon	Method	Unique rate	ELM < 10	Neutrality	ElecNeg	$E_f < 0.0$ eV	Screened rate	ΔT_c Top-30 (K)
LaNiAsO	KIAGO	0.94	1.00	0.73	0.58	0.98	0.57	97.64
	SD	1.00	0.50	0.08	0.01	0.96	0.01	−1.42
	SD w/ CG	1.00	0.49	0.08	0.01	0.97	0.01	−0.48
	C-ES	0.89	1.00	0.99	0.84	1.00	0.84	16.79
SrFe _{1.88} Ni _{0.12} As ₂	KIAGO	0.99	1.00	0.79	0.59	0.64	0.37	86.77
	SD	1.00	0.46	0.05	0.00	0.21	0.00	26.76
	SD w/ CG	1.00	0.49	0.04	0.01	0.23	0.00	0.74
	C-ES	0.48	1.00	0.98	0.72	0.24	0.19	18.96
Sr ₄ V ₂ Fe ₂ As ₂ O ₆	KIAGO	0.91	1.00	0.70	0.60	0.91	0.55	89.89
	SD	1.00	0.12	0.29	0.05	0.51	0.01	−13.77
	SD w/ CG	1.00	0.02	0.25	0.02	0.61	0.00	−3.99
	C-ES	0.85	1.00	1.00	0.96	1.00	0.96	−0.00
LaPt ₂ B ₂ C	KIAGO	0.95	1.00	0.71	0.51	0.96	0.49	86.39
	SD	1.00	0.52	0.06	0.01	0.87	0.01	−5.01
	SD w/ CG	1.00	0.38	0.08	0.02	0.90	0.01	−5.27
	C-ES	0.89	1.00	0.75	0.53	0.65	0.22	5.06
HgBa ₂ Ca ₂ Cu ₃ O ₈	KIAGO	0.74	1.00	0.65	0.55	0.96	0.54	16.70
	SD	1.00	0.57	0.00	0.00	1.00	0.00	−29.43
	SD w/ CG	1.00	0.58	0.01	0.00	1.00	0.00	−21.36
	C-ES	0.87	1.00	0.99	0.93	1.00	0.93	1.00
CeBiS ₂ O	KIAGO	0.81	1.00	0.63	0.53	0.88	0.47	94.89
	SD	1.00	0.21	0.14	0.01	0.23	0.00	N/A
	SD w/ CG	1.00	0.05	0.31	0.08	0.22	0.00	N/A
	C-ES	0.85	1.00	1.00	0.94	0.49	0.48	0.42
Bi ₂ Sr ₂ CuO ₆	KIAGO	0.81	1.00	0.68	0.57	0.95	0.55	127.33
	SD	1.00	0.76	0.01	0.01	1.00	0.01	18.34
	SD w/ CG	1.00	0.76	0.01	0.00	1.00	0.00	14.38
	C-ES	0.88	1.00	0.99	0.94	1.00	0.94	52.25
TlSr ₂ CaCu ₂ O ₇	KIAGO	0.74	1.00	0.67	0.57	0.94	0.55	74.64
	SD	1.00	0.67	0.01	0.01	1.00	0.00	5.21
	SD w/ CG	1.00	0.70	0.01	0.00	1.00	0.00	11.53
	C-ES	0.87	1.00	0.99	0.94	1.00	0.94	34.07

Table S.5.2: “Keeping remaining atoms” is the percentage of generated compositions in which the designated set of elements and their compositions are preserved within a 1% error (e.g., In the top row of the table, the composition of $\text{FeAsF}_{0.2}\text{O}_{0.8}$ in $\text{CeFeAsF}_{0.2}\text{O}_{0.8}$.) “Keeping sum of substitute atoms” is the percentage in which the total substituted composition—excluding the designated elements and compositions—matches the targeted substituted element’s composition within 1% error (e.g., In the top row of the table, the composition of Ce^{+3} in $\text{CeFeAsF}_{0.2}\text{O}_{0.8}$.). Other metrics follow the definitions in Table S.5.1.

Base materials from SuperCon	Substitute target	Method	Unique rate	ELM < 10	Neutrality	ElecNeg	$E_f < 0.0$ eV	Keeping sum of substitute atoms	Keeping remain atoms	Screening rate	ΔT_c Top-30 (K)
$\text{CeFeAsF}_{0.2}\text{O}_{0.8}$	Ce^{+3}	KIAGO	0.99	1.00	1.00	0.26	0.99	1.00	1.00	0.25	14.53
		SD	1.00	0.40	0.03	0.01	0.54	0.00	0.13	0.00	N/A
		SD w/ CG	1.00	0.34	0.03	0.01	0.47	0.00	0.13	0.00	N/A
		C-ES	0.81	1.00	1.00	0.45	0.94	1.00	1.00	0.42	9.99
$\text{LaFeAsO}_{1.0}$	La^{+3}	KIAGO	1.00	1.00	1.00	0.09	1.00	1.00	1.00	0.09	35.62
		SD	1.00	0.45	0.02	0.01	0.58	0.04	0.18	0.00	1.24
		SD w/ CG	1.00	0.39	0.01	0.00	0.51	0.04	0.18	0.00	N/A
		C-ES	0.85	1.00	1.00	0.41	0.98	1.00	1.00	0.39	29.45
SrFe_2As_2	Sr^{+2}	KIAGO	1.00	1.00	1.00	0.17	0.26	1.00	1.00	0.06	29.35
		SD	1.00	0.52	0.03	0.00	0.21	0.04	0.15	0.00	N/A
		SD w/ CG	1.00	0.44	0.07	0.01	0.20	0.05	0.13	0.00	N/A
		C-ES	0.87	1.00	1.00	0.34	0.23	1.00	1.00	0.09	13.78
$\text{Bi}_2\text{CaSr}_2\text{Cu}_2\text{O}_8$	Bi^{+3}	KIAGO	0.96	1.00	1.00	1.00	1.00	1.00	1.00	1.00	14.61
		SD	1.00	0.70	0.01	0.01	1.00	0.41	0.56	0.00	0.15
		SD w/ CG	1.00	0.65	0.01	0.01	1.00	0.39	0.52	0.00	0.42
		C-ES	0.82	1.00	1.00	0.94	1.00	1.00	1.00	0.94	6.42
CeNiC_2	Ce^{+4}	KIAGO	0.99	1.00	1.00	0.40	1.00	1.00	1.00	0.40	17.30
		SD	1.00	0.72	0.07	0.03	0.98	0.02	0.04	0.00	N/A
		SD w/ CG	1.00	0.77	0.06	0.02	0.98	0.02	0.04	0.00	N/A
		C-ES	0.88	1.00	1.00	0.55	0.93	1.00	1.00	0.50	6.26
LaNiC_2	La^{+3}	KIAGO	1.00	1.00	1.00	0.82	1.00	1.00	1.00	0.82	25.24
		SD	1.00	0.76	0.03	0.01	0.98	0.07	0.12	0.00	N/A
		SD w/ CG	1.00	0.76	0.04	0.01	0.98	0.07	0.11	0.00	0.12
		C-ES	0.88	1.00	1.00	0.70	0.93	1.00	1.00	0.64	7.55
MgCoNi_3	Co^{+2}	KIAGO	1.00	1.00	1.00	0.96	0.00	1.00	1.00	0.00	N/A
		SD	1.00	0.42	0.71	0.65	0.36	0.01	0.02	0.00	N/A
		SD w/ CG	1.00	0.42	0.64	0.59	0.38	0.01	0.02	0.00	N/A
		C-ES	0.88	1.00	1.00	0.35	0.24	1.00	1.00	0.07	-2.41
$\text{RuSr}_2\text{GdCu}_2\text{O}_8$	Sr^{+2}	KIAGO	0.95	1.00	1.00	1.00	1.00	1.00	1.00	1.00	-33.66
		SD	1.00	0.55	0.05	0.04	1.00	0.13	0.21	0.00	-0.23
		SD w/ CG	1.00	0.57	0.05	0.04	1.00	0.14	0.22	0.00	-0.08
		C-ES	0.81	1.00	1.00	0.90	1.00	1.00	1.00	0.90	3.70
$\text{RuSr}_2\text{YCu}_2\text{O}_8$	Y^{+3}	KIAGO	0.85	1.00	1.00	1.00	1.00	1.00	1.00	1.00	46.16
		SD	1.00	0.65	0.08	0.06	1.00	0.09	0.29	0.00	-0.89
		SD w/ CG	1.00	0.64	0.07	0.05	1.00	0.12	0.28	0.00	2.02
		C-ES	0.81	1.00	1.00	0.94	1.00	1.00	1.00	0.94	37.60
$\text{Y}_2\text{Fe}_3\text{Si}_5$	Y^{+3}	KIAGO	1.00	1.00	1.00	0.67	1.00	1.00	1.00	0.67	7.56
		SD	1.00	0.33	0.18	0.05	0.56	0.03	0.05	0.00	N/A
		SD w/ CG	1.00	0.31	0.21	0.07	0.58	0.03	0.04	0.00	N/A
		C-ES	0.87	1.00	1.00	0.16	1.00	1.00	1.00	0.16	1.45
YIrSi	Y^{+3}	KIAGO	1.00	1.00	1.00	0.02	1.00	1.00	1.00	0.02	5.08
		SD	1.00	0.90	0.28	0.06	0.70	0.02	0.04	0.00	3.42
		SD w/ CG	1.00	0.90	0.30	0.07	0.72	0.02	0.03	0.00	-1.43
		C-ES	0.87	1.00	1.00	0.34	0.99	1.00	1.00	0.34	5.31